THE JOURNAL OF PHYSICAL CHEMISTRY C

Article

pubs.acs.org/JPCC

Growth of Bi_2O_3 Ultrathin Films by Atomic Layer Deposition

Y. D. Shen,[†] Y. W. Li,*[,†] W. M. Li,[‡] J. Z. Zhang,[†] Z. G. Hu,[†] and J. H. Chu[†,§]

[†]Key Laboratory for Polar Materials and Devices of Ministry of Education, East China Normal University, Shanghai 200241, People's Republic of China

[‡]Picosun Oy, Masalantie 365, 02430 Masala, Finland

[§]National Laboratory for Infrared Physics, Shanghai Institute of Technical Physics, Chinese Academy of Sciences, Shanghai 200083, People's Republic of China

ABSTRACT: Bismuth trioxide (Bi_2O_3) ultrathin films were successfully synthesized on silicon substrates by means of atomic layer deposition (ALD) using $Bi(thd)_3$ (thd: 2,2,6,6-tetramethyl-3,5-heptanedionato) and H_2O as precursors. The optimum ALD window was about 270−300 °C, and an ALD-type growth mechanism via surface saturation reaction was identified; the growth rate was about 0.1 Å/cycle. The X-ray diffraction and high-resolution transmission electron microscopy investigation revealed that Bi_2O_3 films crystallized into a predominant alpha phase above 250 °C. The resistivity at room temperature was about 1.2×10^6 Ω·cm, which is also proof of the α-phase of as-deposited Bi_2O_3 films. In addition, a new method to obtain γ-Bi_2O_3 film was discovered. The α-Bi_2O_3 films (synthesized by ALD) transformed into metastable γ-Bi_2O_3 with preferred orientation (222) after annealing above 512 °C, and γ-phase could persist at room temperature.

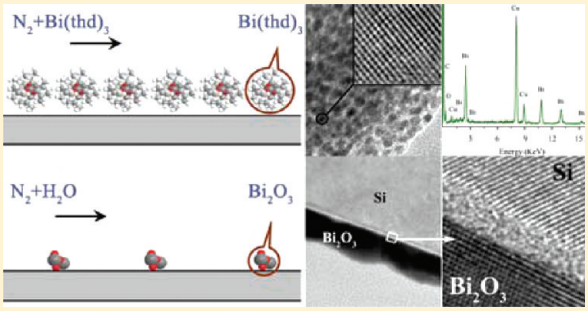

I. INTRODUCTION

Bismuth trioxide (Bi_2O_3) is an interesting material with many promising applications. It has high refractive index and dielectric permittivity, optical nonlinearity, and ultrafast response, as well as marked photoconductivity and photoluminescence.[1−3] These unique characteristics make Bi_2O_3 a suitable candidate for several applications such as heterogeneous catalysts, sensors, microelectronics, optical coatings, blue laser recording, and glass manufacturing.[4−9]

Bi_2O_3 is known to have the four polymorphic forms of α, β, γ, and δ.[5] The monoclinic α-Bi_2O_3 phase is a thermodynamically stable polymorph below 729 °C. It transforms to the fluorite-type δ-Bi_2O_3 phase above 730 °C and remains stable up to the melting point at 825 °C. The tetragonal β-Bi_2O_3 phase and the cubic γ-Bi_2O_3 phase are metastable polymorphs. δ-Bi_2O_3 plays an important role as an excellent oxide ion conductor in electrochemical cells, and α-Bi_2O_3 is a wide band gap (about 3 eV, dependent on fabrication conditions) p-type semiconductor.[10]

Recently, there has been increasing interest in Bi_2O_3 material for applications of manufacturing sensors, ceramics, and glass. It also has been used for modifying physical properties of other nanocompounds[11] and for developing novel applications.[12−14] Many Bi_2O_3 materials that have been studied were in the form of ceramics, amorphous thin films, or nanostructures, etc.[14−16] Bi_2O_3 thin films have been synthesized previously by pulse laser deposition (PLD),[17] chemical vapor deposition (CVD),[18] reactive ion sputtering,[19] and thermal oxidation of thermally evaporated Bi films;[10] however, most of these films presented nonstoichiometric phases, such as $Bi_2O_{2.33}$ and $Bi_2O_{2.75}$, and even elemental Bi. Due to the low melting point (1097 K),[5] volatility of bismuth, and variation of valence states of bismuth (II, III, and V), it is very difficult to obtain stoichiometric Bi_2O_3 ultrathin films with good crystallinity. Kang et al. obtained stoichiometric Bi_2O_3 film by direct liquid injection (DLI)-metal organic chemical vapor deposition (MOCVD) process with $Bi(thd)_3$ (thd: 2,2,6,6-tetramethyl-3,5-heptanedionato) dissolved in *n*-butylacetate; the film deposited at 300 °C was amorphous, and postannealing temperature of above 550 °C was needed to transform the amorphous film into crystalline with monoclinic α-phase.[20]

Bismuth is also an important component in Bi-based ferroelectric oxides like $BiFeO_3$, $Bi_4Ti_3O_{12}$, and $SrBi_2Ta_2O_9$. The successful synthesis of Bi_2O_3 is an essential requirement for the synthesis of these complex oxides by ALD. Little work has been reported on Bi_2O_3 using ALD.[21] Timo Hatanpää et al. synthesized and evaluated some bismuth alkoxides ($Bi(O^tBu)_3$ (O^tBu = *tert*-butoxide), $Bi(OCMe_2{}^iPr)_3$ (Me = methyl, ^iPr = isopropyl), $Bi(OC^iPr_3)_3$, bismuth β-diketonate, $Bi(thd)_3$, and bismuth carboxylate, $Bi(O_2C^tBu)_3$) as possible precursors for ALD;[21] however, the deposition of Bi_2O_3 film was not further explored. Vehkamäki et al. obtained amorphous BiO_x films by ALD with bismuth tris(bis(trimethylsilyl)amide) ($Bi(N(SiMe_3)_2)_3$), and the films crystallized after postdeposition annealing at 800 °C.[22] Later they employed the same bismuth precursors to prepare Bi−Ti−O films; however, the films were

Received: June 2, 2011
Revised: January 10, 2012
Published: January 13, 2012

   dx.doi.org/10.1021/jp205180p | *J. Phys. Chem. C* 2012, 116, 3449−3456

also amorphous and crystallized by postannealing at 750 °C.[23] To our knowledge, deposition of well-crystalline Bi_2O_3 films has never been carried out via ALD.

Atomic layer deposition (ALD), also known as atomic layer epitaxy (ALE) or atomic layer chemical vapor deposition (ALCVD),[24] is an attractive technology. It has become one of the solutions for the ultrathin films because of its precise control in the film thickness and composition with excellent uniformity, and near perfect conformal step coverage at subnanodimension. Unlike other thin film deposition techniques, such as sol−gel, PLD (pulse laser deposition), sputtering, and CVD (chemical vapor deposition), ALD employs self-limiting surface reactions that result in the growth of one atomic layer (or less) per ALD cycle, and high-quality thin films are achieved layer by layer with precisely controlled film thickness to single atomic layer or angstrom scale and excellent conformity in very high aspect ratio geometries and porous structures. Moreover, ALD deposition can be performed at much lower temperature than some other techniques, and lower deposition temperature with high quality is desired for manufacture of silicon-based integrated circuits.

In this work, we report preparation of good-crystalline α-Bi_2O_3 ultrathin films by ALD with $Bi(thd)_3$ and H_2O. The molecular structure of $Bi(thd)_3$, growth rate, growth mechanism, electrical resistivity of Bi_2O_3 films, and influences of postannealing temperature were studied.

II. EXPERIMENTAL SECTION

The Bi_2O_3 ultrathin films were synthesized on silicon substrates by ALD (Sunale R-75, Picosun Oy) process. $Bi(thd)_3$ (min. 98% (99.9%-Bi), Strem Ltd.) and deionized water were used as bismuth and oxygen precursor, respectively. High-purity nitrogen (99.9995%) was used as the sources carrier and purging gas. Prior to the Bi_2O_3 film deposition, the Si(100) substrates were precleaned by alcohol and deionized water. No extra processes were carried out to remove the ultrathin natural oxide layer at the surface of the silicon wafer. $Bi(thd)_3$ was evaporated from a booster bottle held at 190 °C. The H_2O vapor was generated in a liquid-source bottle at room temperature. During the deposition process, the reactor pressure was controlled at about 6−15 hPa. Within each ALD cycle, $Bi(thd)_3$ and H_2O vapor were introduced alternately into the reaction chamber with N_2 carrier gas, and each precursor pulse was separated with N_2 as a purging step. The carrier gas flow rate for bismuth precursor and water was 150 and 200 sccm (standard cubic centimeters per minute), respectively. Experimental conditions for the ALD deposition of Bi_2O_3 films are summarized in Table 1. The cycles and deposition temperature dependences of the film thickness were also studied in detail.

The crystalline structure and growth rate of Bi_2O_3 films deposited under various temperatures were studied. The effect of thermal treatment on the crystallization behavior of the Bi_2O_3 film was also investigated. The films were postannealed for 600 s in air atmosphere using a rapid thermal annealing (RTA) furnace at 400, 500, 600, and 700 °C, respectively. The as-deposited and RTA samples were denoted by A, B, C, D, and E, respectively. To compare Bi_2O_3 films with Bi_2O_3 powder and determine the crystalline structure of Bi_2O_3 films, $Bi(thd)_3$ was added into pure water to allow complete reaction and evaporated to obtain Bi_2O_3 powder.

The thermal gravimetric analysis/differential thermal analysis (TGA/DTA) measurements for $Bi(thd)_3$ and Bi_2O_3 powder were carried out with a Metter-Toledo TGA/SDTA 851e thermal gravimetric analyzer. The thicknesses of the films grown on Si substrates were measured by a spectroscopic ellipsometer. The crystalline structure of the films was analyzed by X-ray diffraction (XRD) with Cu Kα radiation (λ = 1.5406 Å) at a step of 0.02 in the range 10−65°. The microstructure of the as-prepared sample was analyzed by high-resolution transmission electron microscopy (HRTEM, JEOL JEM-2100F) with 200 KV accelerating voltage and energy-dispersive X-ray spectroscopy (EDS) attached to the JEM-2100F. In addition, the films are also deposited on the SiO_2/Si substrates for electric measurements. The electrical conductivity of Bi_2O_3 films was measured by electrometer (Kethley 6517A). The film topographic information, roughness, and grain size were studied using an NT-MDT Solver P47-PRO scanning probe microscope operating in the contact atomic force microscope (AFM) mode. All measurements (except for TGA/DTA) were carried out at room temperature/pressure.

Table 1. Operating Conditions for Deposition of Bi_2O_3 Films

substrates temperature	200−350 °C
Bi-source precursor	$Bi(thd)_3$
O-source precursor	H_2O
carrier gas	99.9995% N_2
$Bi(thd)_3$ carrier gas flow	200 sccm
$Bi(thd)_3$ source temperature	190 °C
$Bi(thd)_3$ pulse time	0.2−10 s
$Bi(thd)_3$ purging time	5 s
H_2O c gas flow	200 sccm
H_2O source temperature	room temperature
H_2O pulse time	0.2 s
H_2O purging time	4 s

III. RESULTS AND DISCUSSION

Structure and Thermal Characteristics of the $Bi(thd)_3$ Molecule. $Bi(thd)_3$, whose chemical formula is $C_{33}H_{57}O_6Bi$, has been used in MOCVD technology as a bismuth precursor.[18] However, there are no reports that it is used for ALD, and its structure has not been reported previously.[19] Its melting point is 114−116 °C, and its boiling point is 295 °C (supported by Strem Ltd.). The molecule structure of $Bi(thd)_3$ is shown in Figure 1. The molecule is monomeric containing three chelating [2,2,6,6-tetramethyl-3,5-heptanedionato] ligands. Important bond lengths and angles are summarized in Table 2. The length of Bi−O σ-bonds are in the range of 1.108−1.132 Å, and the angles between Bi−O σ-bonds are close to 90°, but the other angles between the dative Bi−O bonds are slightly wider (99−113°). Obviously, a distorted octahedron of oxygen atoms around the central Bi^{3+} forms in the molecule.

In order to investigate the volatility and thermal stability of $Bi(thd)_3$, TGA/DTA measurement for $Bi(thd)_3$ was carried out, and the TGA and DTA thermograms of the $Bi(thd)_3$ compound are shown in Figure 2a; the inset is the photograph of Bi_2O_3 powder obtained by $Bi(thd)_3$ decomposed at 450 °C. Analysis of the TGA thermograms revealed that residues at 600 °C were 32.6%, and it approximated the computational result (30.7%, the molecular weight ratio of $BiO_{1.5}$ to $Bi(thd)_3$). The fine distinction may attributed to the moisture sensitivity, the exposure to ambient air before loading into the crucible, causing a small amount of Bi_2O_3 produced that increased

dx.doi.org/10.1021/jp205180p | J. Phys. Chem. C 2012, 116, 3449−3456

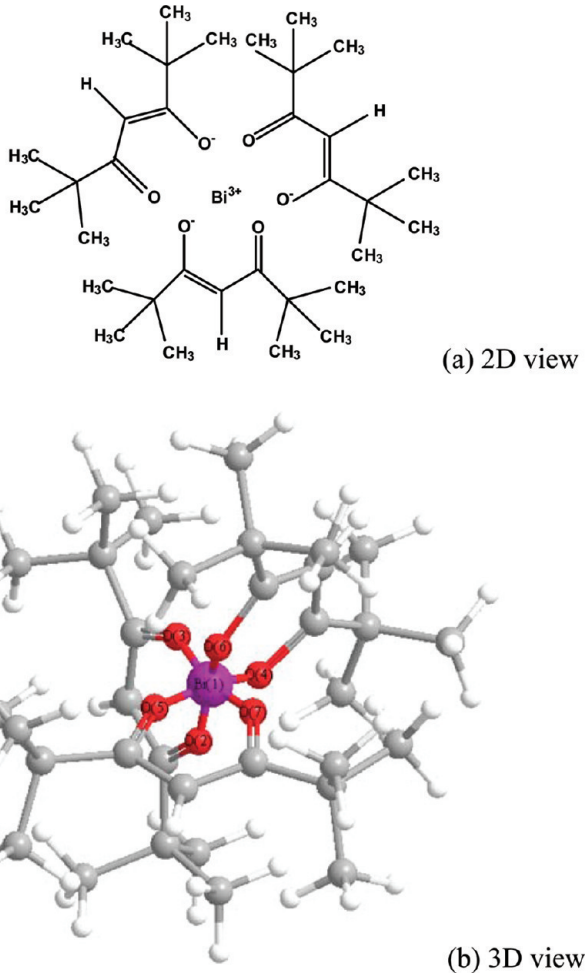

Figure 1. Molecule structure of $Bi(thd)_3$: (a) 2D view, (b) 3D view. Note that the purple, red, gray, and white balls denote bismuth, oxygen, carbon, and hydrogen atoms, respectively.

Table 2. Selected Bond Lengths (Å) and Angles (deg) for $Bi(thd)_3$

Bi(1)−O(2)	1.109
Bi(1)−O(3)	1.108
Bi(1)−O(4)	1.115
Bi(1)−O(5)	1.126
Bi(1)−O(6)	1.116
Bi(1)−O(7)	1.132
O(2)−Bi(1)−O(3)	113
O(2)−Bi(1)−O(4)	89
O(2)−Bi(1)−O(7)	90
O(2)−Bi(1)−O(5)	73
O(3)−Bi(1)−O(4)	90
O(3)−Bi(1)−O(6)	89
O(3)−Bi(1)−O(5)	91
O(4)−Bi(1)−O(6)	110
O(4)−Bi(1)−O(7)	88
O(6)−Bi(1)−O(7)	70
O(5)−Bi(1)−O(7)	99
O(5)−Bi(1)−O(6)	89

weight of residues of the experimental results as compared to the computational value. The TGA curve indicates that $Bi(thd)_3$ has good thermal stability and decomposes to Bi_2O_3 at about 360 °C. The exothermic maxima at about 512 °C

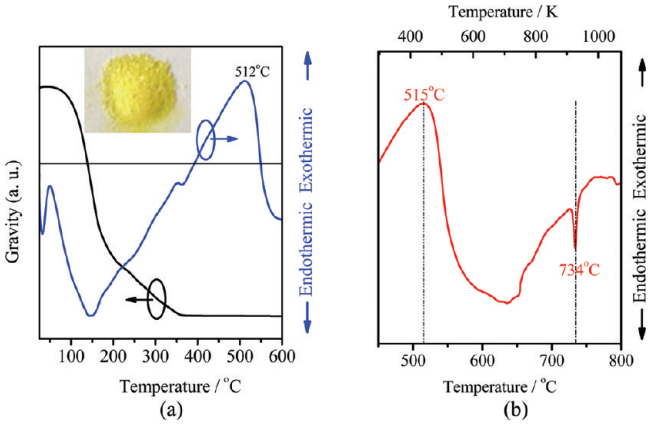

Figure 2. (a) TGA/DTA thermograms of the $Bi(thd)_3$ powder. The blue lines denote the DTA diagrams, and the red line denotes the TGA curves. The inset is the photograph of Bi_2O_3 powder obtained by $Bi(thd)_3$ thermal decomposed at 450 °C. (b) DTA thermograms of the Bi_2O_3 powder.

imply that Bi_2O_3 has a structural phase transition. This result is in accordance with analysis of XRD patterns as shown below (Figure 7).

The DTA thermogram of the as-prepared Bi_2O_3 powder is shown in Figure 2b. The same exothermic peak is present, and it also implies that the $Bi(thd)_3$ decomposes to Bi_2O_3 above 360 °C. Moreover, the endothermic peak at about 734 °C indicates that Bi_2O_3 transforms into δ-Bi_2O_3.[25]

Figure 3 shows the $Bi(thd)_3$ partial pressure vs evaporation temperature. The values of pressure were obtained by the

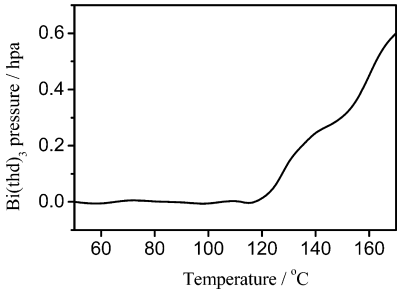

Figure 3. Curve of $Bi(thd)_3$ partial pressure vs temperature.

pressure sensors in the ALD system. Obviously, the Bi-precursor partial pressure increases with the temperature rise (above 120 °C). The selection of Bi-source evaporation temperature 190 °C is reasonable for ALD.

The thermal stability of $Bi(thd)_3$ may be attributed to these rather stable Bi−O σ-bonds. On the other hand, the dative Bi−O bonds in $Bi(thd)_3$ have rather strong polarity, which results in its high sensitivity to polarity molecule H_2O; therefore, $Bi(thd)_3$ shows reactivity against water.[19]

Reaction Mechanism for $Bi(thd)_3$ and H_2O. H_2O, as a polar molecule, may cause the dative Bi−O bond break. H^+ and OH^- combine with the O^- and Bi^{3+}, respectively. The $Bi(thd)_3$ molecules decomposes and transient intermediate $Bi(OH)_3$ forms, while $Bi(OH)_3$ is quite unstable and decomposes into Bi_2O_3 and H_2O (above 100 °C at room pressure). The whole reaction can be described as below.

$$2Bi(thd)_3 + 3H_2O \rightarrow Bi_2O_3 + 6Hthd \quad (1)$$

dx.doi.org/10.1021/jp205180p | J. Phys. Chem. C 2012, 116, 3449−3456

In fact, the Bi_2O_3 powder was also obtained by reaction of $Bi(thd)_3$ and deionized water, and it shows the same appearance (inset in Figure 2a).

The chemistry of the $Bi(thd)_3/H_2O$ ALD process should described by the two successive "half-reactions", presented in the following equations

$$\| Bi{-}OH + Bi(thd)_3(g) \rightarrow \| Bi{-}O{-}Bi(thd)_2 + Hthd \quad (2)$$

$$\| Bi{-}thd + H_2O(g) \rightarrow \| Bi{-}OH + Hthd \quad (3)$$

where || denotes solid surface and g denotes gas. Actually, the $Bi(thd)_3/H_2O$ process may be more complex than revealed by eqs 3 and 4. For example, one $Bi(thd)_3$ molecule may combine with more than one hydroxyl group (−OH) in eq 2.

Growth Characteristics of Bi_2O_3 Films. In order to evaluate the ALD window, Bi_2O_3 films were deposited in the temperature range from 200 to 350 °C. The $Bi(thd)_3$ pulse time was fixed at 6 s (the reason is mentioned below). The Bi_2O_3 thin films exhibit light yellow color (inset of Figure 5). Figure 4 shows the dependence of growth per cycle (GPC) on

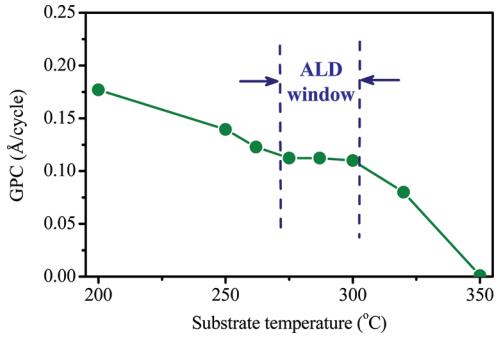

Figure 4. Thickness of Bi_2O_3 films on Si(100) (black ●) versus deposition temperature (1000 cycles) using the $Bi(thd)_3$ pulse time 2 s. Potential ALD window for Bi_2O_3 growth is indicated.

deposition temperature. The GPC at 200 °C is about 0.18 Å/cycle, and it decreases to about 0.1 Å/cycle under 270−300 °C. The GPC was observed almost to be independent of the deposition temperature range from 270 to 300 °C. At 350 °C, the Bi_2O_3 films could not be successfully synthesized, and the GPC reduces to zero. Therefore, the ALD window should be 270−300 °C. The excessive growth rate at a lower process temperature may result from multilayer adsorption because of $Bi(thd)_3$ condensing. On the other hand, decreasing of growth rate at higher temperature may be attributed to $Bi(thd)_3$ desorption from the solid surface.[24,26] Additionally, the GPC slightly decreases with temperature in the ALD window because the increasing temperature decreases the number of reactive surface sites.[27]

The film thickness as a function of deposition cycles was checked in detail at a reaction temperature of 278(±5) °C. Figure 5 reveals the linear growth as a function of the number of ALD cycles on Si(100). The linearity indicates that the thickness of Bi_2O_3 films can be precisely controlled by number of ALD cycles. The horizontal axis offset in the relative thickness suggests a 40-cycle nucleation delay on Si(100).

The dependence of thicknesses on Bi-precursor pulse time was investigated. Films were synthesized with various Bi-precursor pulse times, and the water pulse length was always

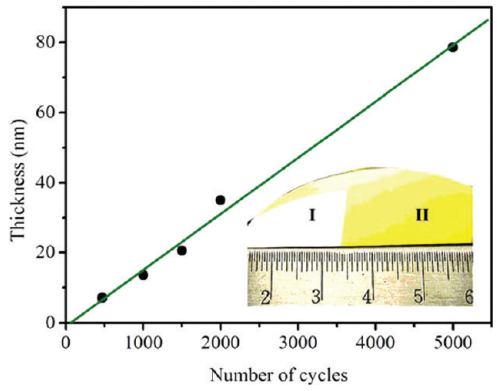

Figure 5. Thickness of Bi_2O_3 films on Si(100) (black ●) versus number of $Bi(thd)_3$ cycles at 278(±5) °C using the $Bi(thd)_3$ pulse time 2 s. The solid lines are the best linear fit to the data. Photograph of the Bi_2O_3 film grown on Si at 280 °C (2000 ALD cycles). The inset is a photograph of Bi_2O_3 film. The white region (I) is uncovered Si substrate; a polished Si wafer masked it during the deposition, and the light yellow region (II) indicates Bi_2O_3 film.

kept at 0.2 s. The selection of the water pulse time was based on our previous study that fully saturated H_2O pulse was at 0.1 s. In all cases, a fixed ALD cycle (1000 cycles) was done, and the film thicknesses were measured using spectroscopic ellipsometry. Figure 6 shows the dependence of the growth

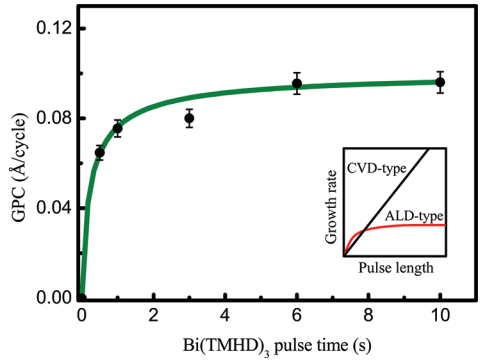

Figure 6. Growth rate of Bi_2O_3 as a function of the $Bi(thd)_3$ pulse time at 290 °C on silicon; $Bi(thd)_3$ temperature is 190 °C. The film thickness was measured by ex situ spectroscopic ellipsometry. The inset shows the ideal ALD-type and CVD-type growth rate.

rate on the $Bi(thd)_3$ pulse time at a deposition temperature of 290 °C. Note that the $Bi(thd)_3$ vaporization temperature was 190 °C. It shows the nonlinear relation of pulse time and growth rate. The growth rate increases with an increasing $Bi(thd)_3$ pulse time and then reaches a saturation value of about 0.1 Å/cycle since the pulse time is longer than 6 s, indicating a self-limiting growth process characteristic of ALD. The behavior of the growth rate with respect to the precursor pulse length was very different from chemical vapor deposition (CVD)-type growth. In a typical CVD process, the film growth rate is in direct proportion to precursor pulse time, as show in the inset of Figure 6. In contrast, the growth rate of ALD will reach saturation due to the self-limiting effect. The growth rate fits well to a Langmuir adsorption model.[28] The results imply that the films are not grown via the CVD growth mechanism but via ALD-type.

The growth rate 0.1 Å/cycle is approximate to the report,[29] and this value is much lower than those of other materials, such

dx.doi.org/10.1021/jp205180p | J. Phys. Chem. C 2012, 116, 3449−3456

as $Zn(C_2H_5)_2$ for ZnO (1.8 Å/cycle),[30] $Gd((^iPrN)_2CNMe_2)_3$ for Gd_2O_3 (1.1 Å/cycle),[31] $Ta(OC_2H_5)_5$ for Ta_2O_5 (0.8 Å/cycle),[32] $CpHf(NMe_2)_3$ for HfO_2 (0.8 Å/cycle),[33] and $TiCl_4$ for TiO_2 (0.5 Å/cycle).[34] Obviously, the film thickness obtained per cycle is also less than the lattice constant (for α-Bi_2O_3, a = 5.848 Å, b = 8.166 Å, 7.509 Å; JCPDF 712274), which implies a full Bi_2O_3 monolayer cannot be grown in one ALD cycle. The low growth rate is attributed to following possible reasons.

First, the bulky ligands of $Bi(thd)_3$ may cause marked steric hindrance.[27,35] The size of the $Bi(thd)_3$ molecule is rather large (the diameter of the $Bi(thd)_3$ molecule is larger than 10 Å), which results in a low coverage factor of Bi^{3+} occupation on the surface. The schematic drawing of one ALD cycle is shown in Figure 7. Evidently, low coverage factor will result in low GPC.

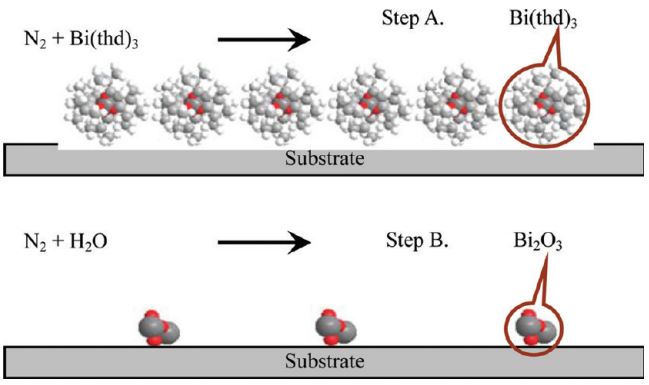

Figure 7. Sketch of one ALD cycle process for Bi_2O_3.

Similar precursors ($M(thd)_n$, M denotes metal) of this effect has been reported.[36,37] It is worth mentioning that almost all such similar precursors with thd ligands bring exceptionally low growth rate for ALD processes.[27] Table 3 summarizes some metal oxides GPC growth by ALD using $M(thd)_n$ (n = 1, 2, 3, 4) precursors. It shows that this type of precursor usually bring a low growth rate. In fact, Deepatana et al. had theoretically and experimentally studied the steric hindrance effect.[38,39]

Second, the adsorption mechanism may affect the GPC. It was possible that $Bi(thd)_3$ nonpolar molecules adsorb both physically and chemically on the surface of the substrate. When adsorption and desorption reach equilibrium at a certain temperature, the adsorbate ($Bi(thd)_3$) could not occupy all sites and form an entire monolayer, which may result in the reduction of GPC. No Bi_2O_3 film was observed on the silicon substrate at deposition temperature of 350 °C, which implies that physisorption become extremely weak due to thermodynamic motivation at the high temperature 350 °C. This behavior is different from chemical adsorption; chemical decomposition would result in excessive film growth rate.[24]

Fortunately, the films needed for very deep submicrometer integrated circuits are ultrathin, and thus the slowness of ALD is not an important issue.[34] Furthermore, in a special ALD process, $M(thd)_n$ alkoxide was selected due to its reasonably low growth rate matching the low growth rate of other precursors. Matching of the deposition rates can fabricate the desired stoichiometric films; for example, Harjuoja et al. successfully synthesized $PbZrO_3$ films by ALD with Ph_4Pb and $Zr(thd)_4$.[40] $Bi(thd)_3$ may be a candidate for growth of Bi-based complex oxide films by ALD, such as $BiFeO_3$. Further such research will be the subject of another work.

Crystalline Structure and Morphology of Bi_2O_3 films. XRD patterns are shown in Figure 8. The Bi_2O_3 film deposited

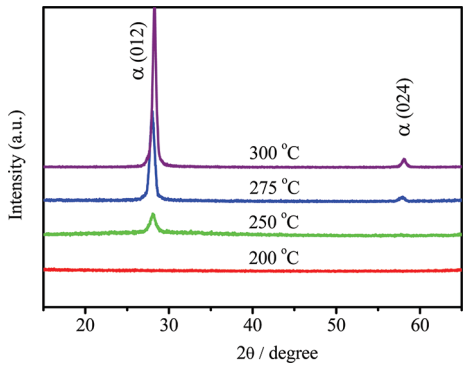

Figure 8. XRD patterns for Bi_2O_3 films deposited on Si(100) as a function of deposition temperature at temperature 200, 250, 275, and 300 °C, respectively).

at 200 °C is amorphous. Above 250 °C, the films crystallized into low-temperature stable α-phase, and the films grow in the orientation of (012) (consistent with JCPDF card 712274). The crystallinity of Bi_2O_3 films improves with the increasing deposition temperature.

The crystalline structure of the Bi_2O_3 film was verified further by high-resolution transmission electron microscopy (HRTEM). Figure 9a shows that the Bi_2O_3 film (deposited at 250 °C) is α-phase polycrystalline/amorphous mixed structure. The inset of Figure 9a shows the typical HRTEM image of a Bi_2O_3 crystalline grain; a lattice space with value of about 0.317 nm was measured, which corresponds to the (012) plane of monoclinic α-Bi_2O_3. From the corresponding EDS analysis (Figure 9b), the body of the film is composed of Bi and O, and the ratio of Bi to O approximates to 2:3, which conform to the chemical formula of Bi_2O_3. The Cu and C elements (marked in the EDS spectrum) originate from the TEM copper grid and carbon support film, respectively. Figure 9c shows that the 290 °C as-deposited Bi_2O_3 film crystallized into α-phase completely. About 1.5 nm thickness natural oxide layer (SiO_2) on the silicon substrate can be observed. Obviously, parts a and c of Figure 9 imply that the higher deposition temperature would improve the crystallization of the films. The analysis of HRTEM is in accordance with the results from XRD. A clear interface of substrate/Bi_2O_3 was observed in Figure 9d, and the subsequent Bi_2O_3 crystallizes into α-phase completely, which

Table 3. Growth Rate of Some Metal Oxides Growth by ALD Using $M(thd)_n$ Precursors (M = Bi, La, Fe, Zr, etc., n = 1, 2, 3, 4)

precursor	$Bi(thd)_3$	$Li(thd)$	$La(thd)_3$	$Fe(thd)_3$	$Zr(thd)_4$
growth rate (Å/cycle)	0.1[a]	<0.32[b,53]	0.26[b,54]	0.1[55]	0.1[b,40]
precursor	$Er(thd)_3$	$Gd(thd)_3$	$Dy(thd)_3$	$Lu(thd)_3$	$Co(thd)_2$
growth rate (Å/cycle)	0.19[b,54]	0.21[b,54]	0.19[b,54]	0.18[b,54]	0.2[56]

[a]This work. [b]Binary/ternary metal oxides. The virtual growth rate of monometal oxides must be less than the value listed in this table.

dx.doi.org/10.1021/jp205180p | J. Phys. Chem. C 2012, 116, 3449–3456

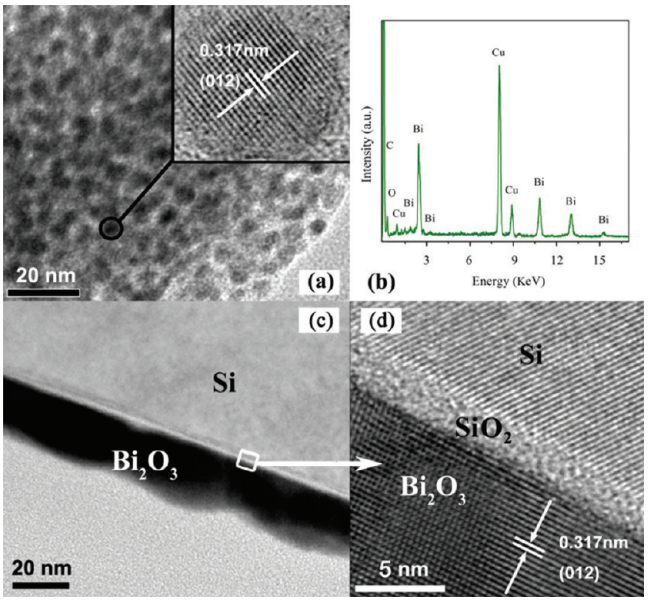

Figure 9. (a) TEM image of Bi_2O_3 film (deposited at 250 °C); HRTEM image enlarging the selected part in (a). (b) EDS spectrum of the Bi_2O_3 film. The Cu and C shown in the spectrum originate from the TEM Cu grid and carbon support film, respectively. The TEM sample was scratched by a sharp blade from the as-prepared Bi_2O_3 film. (c) Cross-sectional TEM image of Bi_2O_3 film (deposited at 290 °C). (d) HRTEM image enlarging the selected part in (c).

implies that the crystallization of Bi_2O_3 film starts at the interface.

Raman scattering investigation also indicates the α-phase of as-deposited Bi_2O_3 films (above 250 °C) and increasing crystallization with the increasing deposition temperature (not shown here), which are consistent with analysis of XRD and HRTEM.

The crystalline Bi_2O_3 film was obtained via ALD though the deposition temperature is lower than that by CVD. Based on the theory for kinetics of crystal film growth,[41,42] the adatoms at the substrate surface need a certain activated energy to diffuse to the local equilibrium sites and then rearrange orderly. Adatom diffusion is derived from considering a random walk in two dimensions, and the adatom average migration time can be estimated by[41,42]

$$\tau_s = \frac{1}{\nu_s}\exp(\Delta G_s/kT) \quad (4)$$

where ν_s is the vibrating frequency of adatom, ΔG_s is the activated energy, k is the Boltzmann constant, and T is the thermodynamic temperature.

To crystallize the deposited monoatom layer, the migration time (τ_s) and deposition velocity (R) follow the relation $\tau_s \leq 1/R$. Based on the above relation and eq 4, the crystallization temperature may decrease when the deposition velocity is low enough.[41] Usually, ALD deposition velocity is much slower than CVD, which makes the adatoms have a longer time to transit to the equilibrium sites and facilitates an epitaxial film.

As shown in Table 4, some crystalline materials were synthesized by ALD at low temperature but CVD at high temperature. The report is that Bi_2O_3 film prepared by ALD is absent; nevertheless, the crystallization of as-deposited Bi_2O_3 films is reasonable in this work.

Herein the successful synthesis of α-Bi_2O_3 films with $Bi(thd)_3$ by ALD at rather low deposition temperature (below 300 °C) is reported. Although deposition of bismuth oxide films had been previously reported by other researchers, these technologies have their drawbacks, such as requirement of higher temperature (500 °C for thermal oxidation,[10] 800 °C for CVD[43]), presence of nonstoichiometric phases (halide CVD)[18] or mixed phase (MOCVD)[44] amorphous Bi_2O_3 films,[23] etc. To our knowledge, deposition of Bi_2O_3 films with $Bi(thd)_3$ by ALD has never been reported. Some bismuth precursors such as $Bi(O^tBu)_3$, $Bi(OCMe_2{}^iPr)_3$, $Bi(OC^iPr_3)_3$, bismuth β-diketonate, $Bi(thd)_3$, and $Bi(O_2C^tBu)_3$ have been synthesized and evaluated as possible precursors for ALD,[21] but further research of deposition of Bi_2O_3 film is absent. BiI_3, as a halide precursor for CVD or ALD, requires much higher evaporation temperature (280 °C);[43] moreover, the byproduct is corrosive. $Bi(C_6H_5)_3$ is the most commonly used CVD precursor due to its low air and moisture sensitivity; moreover, it has proved to be a more suitable source than classic β-diketonates for DLI-MOCVD of Bi-contained films.[45] Bandoli et al. obtained Bi_2O_3 thin films by MOCVD with $Bi(C_6H_5)_3$, but the phase composition strongly depended on the growth conditions (such as flow rate, pressure).[44] Bedoya et al. studied the decomposition pathways of $Bi(C_6H_5)_3$ occurring in the MOCVD of bismuth oxides and found that deposition temperatures higher than other Bi sources are required.[46] They also compared three different precursors ($Bi(thd)_3$, $Bi(p\text{-tol})_3$, and $Bi(o\text{-tol})_3$) in detail and obtained β-Bi_2O_3 phase by MOCVD with those precursors at 450 °C.[47] $[Bi(N(SiMe_3)_2]_3$ was used for synthesis of BiO_x films via ALD; however, poor reproducibility in the deposition of the binary oxide phase was encountered.[22] $Bi(O^tBu)_3$ has relatively higher vapor pressure than $Bi(thd)_3$, and crystalline Bi_2O_3 films were obtained via MOCVD with $Bi(O^tBu)_3$. The crystalline phase also strongly depended on the growth conditions (such as temperature, flow rate, pressure), and those phases contained not only low-temperature stable α-phase but also high-temperature metastable β- and γ-phase.[48]

The effect of postannealing temperature on the as-deposited films was investigated. Figure 10 shows the XRD patterns of the as-deposited Bi_2O_3 films at 300 °C (a) and samples after post-RTA (rapid thermal annealing) at various temperatures. The XRD patterns suggest that the monoclinic structure started to transform into body-center-cubic structure after post-RTA in the range of 500~600 °C. The phase-transform temperature appears to be consistent with the TGA/DTA results (512 °C) discussed previously as well as in the literature.[5] The diffraction peak positions changed after RTA at 700 °C, corresponding to a preferred orientation (222) and a weaker one of (630) according to JCPDF card 451344. It indicated that the α-phase transformed into the γ-phase at higher annealing temperature.

Table 4. Some Instances of Crystallization Synthesized by ALD/CVD

	Fe_2O_3	ITO	MgO	Gd_2O_3	Co_3O_4
ALD	250 °C[28]	275 °C[57]	150 °C[58]	160–250 °C[31]	138–283 °C[56]
CVD	500 °C[59]	600 °C[60]	400–800 °C[61]	400–600 °C[62]	380–560 °C[63]

dx.doi.org/10.1021/jp205180p | J. Phys. Chem. C 2012, 116, 3449–3456

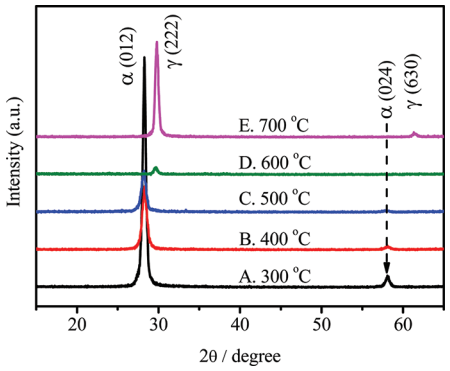

Figure 10. XRD patterns of the Bi_2O_3 films which are as-deposited at temperature 300 °C and post rapid thermal annealed at 400, 500, 600, and 700 °C, respectively.

The electrical conductivity of as-deposited film is about 1.2×10^6 Ω·cm. From the literature,[5] the value that we got is several orders of magnitude less than the electrical conductivity of β-, γ-, and δ-Bi_2O_3 and is in accordance with α-Bi_2O_3. Therefore, the α-phase also can be identified.[5] Note that all the XRD measurements were carried out at room temperature, which means the γ-Bi_2O_3 films can persist to room temperature. From literature, obtaining the "pure" γ-Bi_2O_3 is challenging, and this metastable phase must be stabilized by the addition of another oxide.[49] Our results showed that metastable γ-Bi_2O_3 films can be obtained via thermal annealing of α-phase Bi_2O_3 films.

AFM study was carried out for as-deposited Bi_2O_3 film (290 °C), as shown in Figure 11. The root-mean-square (rms) of the

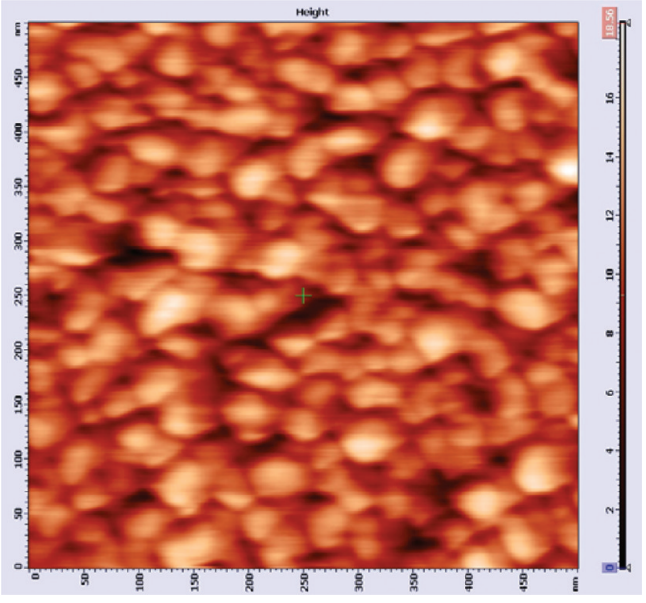

Figure 11. Surface morphology of as-deposited Bi_2O_3 films.

Bi_2O_3 film is about 1.5 nm. The rms value was measured for a scanned area of 0.5×0.5 μm^2, and it was less than the other reports about Bi_2O_3 films (prepared via different methods or on various substrates).[11,20,50−52]

IV. CONCLUSION

Bismuth trioxide (Bi_2O_3) ultrathin films were successfully synthesized on silicon substrates by means of atomic layer deposition using $Bi(thd)_3$ and H_2O as precursor. $Bi(thd)_3$ molecule structure and thermal property as well as ALD reaction mechanism were analyzed. The ALD window is about 270−300 °C. The thickness of Bi_2O_3 films linearly increases with number of ALD cycles. The $Bi(thd)_3$ saturation pulse length was 6 s, and the ALD-type growth mechanism was observed. The growth rate was low, approximately 0.1 Å/cycle. XRD and HRTEM investigations of Bi_2O_3 films show that films crystallized into α-phase above 250 °C . The resistivity at room temperature also proves the α-phase of as-deposited Bi_2O_3 films. The α-Bi_2O_3 films synthesized by ALD started to transform into γ- Bi_2O_3 with preferred orientation (222) above 500 °C and undergo complete transformation after 700 °C RTA. The high-temperature metastable γ-phase can persist at room temperature.

AUTHOR INFORMATION

Corresponding Author

*Phone +86-21-54345123, fax +86-21-54345119, e-mail ywli@ee.ecnu.edu.cn.

Notes

The authors declare no competing financial interest.

ACKNOWLEDGMENTS

We thank Mr. D. W. Cao of Suzhou University for AFM measurements. This work was financially supported by the National Natural Science Foundation of China (Grant Nos. 60906046, 11074076, and 61106122), the State Key Basic Research Program of China (Grant Nos. 2007CB924901 and 2011CB922200), Projects of Science and Technology Commission of Shanghai Municipality (Grant Nos. 10DJ1400200, 10ZR1409800, 09ZZ42, and 10SG28), the Innovation Research Project of East China Normal University, and the Program for Professor of Special Appointment (Eastern Scholar) at Shanghai Institutions of Higher Learning.

REFERENCES

(1) Gobrecht, H.; Seeck, S.; Bergt, H. E.; Martens, A.; Kossmann, K. *Phys. Status Solidi* **1969**, *34*, 569.
(2) Dolocan, V.; Iova, F. *Phys. Status Solidi A* **1981**, *64*, 755.
(3) Leontie, L.; Caraman, M.; Rusu, G. I. *J. Optoelectron. Adv. Mater.* **2000**, *2*, 385.
(4) Matatov-Meytal, Y. I.; Sheintuch, M. *Ind. Eng. Chem. Res.* **1998**, *37*, 309.
(5) Shuk, P.; Wiemhofer, H. D.; Guth, U.; Gopel, W.; Greenblatt, M. *Solid State Ionics* **1996**, *89*, 179.
(6) Peiteado, M.; de la Rubia, M. A.; Velasco, M. J.; Valle, F. J.; Caballero, A. C. *J. Eur. Ceram. Soc.* **2005**, *25*, 1675.
(7) Khonthon, S.; Morimoto, S.; Arai, Y.; Ohishi, Y. *Opt. Mater.* **2009**, *31*, 1262.
(8) Zhi, J.; Geng, Y. Y.; Gu, D. H. *Chin. Opt. Lett.* **2008**, *6*, 294.
(9) Kobayasbhi, K. *J. Non-Cryst. Solids* **2003**, *316*, 403.
(10) Leontie, L.; Caraman, M.; Delibas, M.; Rusu, G. I. *Mater. Res. Bull.* **2001**, *36*, 1629.
(11) Barreca, D.; Rizzi, G. A.; Tondello, E. *Thin Solid Films* **1998**, *333*, 35.
(12) Gou, X.; Li, R.; Wang, G.; Chen, Z.; Wexler, D. *Nanotechnology* **2009**, *20*, 495501.
(13) Yuan, D.; Zeng, J.; Kristian, N.; Wang, Y.; Wang, X. *Electrochem. Commun.* **2009**, *11*, 313.
(14) Zheng, F. L.; Li, G. R.; Ou, Y. N.; Wang, Z. L.; Su, C. Y.; Tong, Y. X. *Chem. Commun.* **2010**, *46*, 5021.
(15) Kim, H. W. *Thin Solid Films* **2008**, *516*, 3665.
(16) Wang, C. H.; Shao, C. L.; Wang, L. J.; Zhang, L.; Li, X. H.; Liu, Y. C. *J. Colloid Interface Sci.* **2009**, *333*, 242.

(17) Leontie, L.; Caraman, M.; Visinoiu, A.; Rusu, G. I. *Thin Solid Films* **2005**, *473*, 230.
(18) Schuisky, M.; Harsta, A. *Chem. Vap. Deposit.* **1996**, *2*, 235.
(19) Fan, H. T.; Teng, X. M.; Pan, S. S.; Ye, C.; Li, G. H.; Zhang, L. D. *Appl. Phys. Lett.* **2005**, 87.
(20) Kang, S. W.; Rhee, S. W. *Thin Solid Films* **2004**, *468*, 79.
(21) Hatanpaa, T.; Vehkamaki, M.; Ritala, M.; Leskela, M. *Dalton Trans.* **2010**, *39*, 3219.
(22) Vehkamaki, M.; Hatanpaa, T.; Ritala, M.; Leskela, M. *J. Mater. Chem.* **2004**, *14*, 3191.
(23) Vehkam ki, M.; Hatanp, T.; Kemell, M.; Ritala, M.; Leskel, M. *Chem. Mater.* **2006**, *18*, 3883.
(24) Suntola, T. *Appl. Surf. Sci.* **1996**, *100*, 391.
(25) Sammes, N. M.; Tompsett, G. A.; Nafe, H.; Aldinger, F. *J. Eur. Ceram. Soc.* **1999**, *19*, 1801.
(26) Putkonen, M.; Niinist, L. *Precursor Chem. Adv. Mater.* **2005**, 125.
(27) Puurunen, R. L. *J. Appl. Phys.* **2005**, 97.
(28) Martinson, A. B. F.; DeVries, M. J.; Libera, J. A.; Christensen, S. T.; Hupp, J. T.; Pellin, M. J.; Elam, J. W. *J. Phys. Chem. C* **2011**, *115*, 4333.
(29) Østereng, E.; Gandrud, K. B.; Nilsen, O.; Fjellvag, H. *BALD2009, book of abstracts*; Uppsala, Sweden, 2009.
(30) Chen, H. C.; Chen, M. J.; Wu, M. K.; Li, W. C.; Tsai, H. L.; Yang, J. R.; Kuan, H.; Shiojiri, M. *IEEE J. Quantum Electron.* **2010**, *46*, 265.
(31) Milanov, A. P.; Xu, K.; Laha, A.; Bugiel, E.; Ranjith, R.; Schwendt, D.; Osten, H. J.; Parala, H.; Fischer, R. A.; Devi, A. *J. Am. Chem. Soc.* **2010**, *132*, 36.
(32) Lintanf-Salaün, A.; Mantoux, A.; Djurado, E.; Blanquet, E. *Microelectron. Eng.* **2010**, *87*, 373.
(33) Niinistö, J.; Mäntymäki, M.; Kukli, K.; Costelle, L.; Puukilainen, E.; Ritala, M.; Leskelä, M. *J. Cryst. Growth* **2010**, *312*, 245.
(34) Hudec, B.; Husekova, K.; Dobrocka, E.; Lalinsky, T.; Aarik, J.; Aidla, A.; Frohlich, K. *IOP Conf. Ser.: Mater. Sci. Eng.* **2010**, *8*, 012024.
(35) Leskelä, M.; Ritala, M. *Angew. Chem., Int. Ed.* **2003**, *42*, 5548.
(36) Ylilammi, M. *Thin Solid Films* **1996**, *279*, 124.
(37) Puurunen, R. L. *Chem. Vap. Deposit.* **2003**, *9*, 327.
(38) Deepatana, A.; Valix, M. *J. Hazard. Mater.* **2006**, *137*, 925.
(39) Deepatana, A.; Valix, M. *Desalination* **2008**, *218*, 297.
(40) Harjuoja, J.; Vayrynen, S.; Putkonen, M.; Niinisto, L.; Rauhala, E. *Appl. Surf. Sci.* **2007**, *253*, 5228.
(41) Tu, K. N.; Mayer, J. W.; Feldman, L. C. *Electronic thin film science: For electrical engineers and materials scientists*; Prentice Hall: Englewood Cliffs, NJ, 1992.
(42) Venables, J. *Introduction to surface and thin film processes*; Cambridge University Press: New York, 2000.
(43) Takeyama, T.; Takahashi, N.; Nakamura, T.; Itoh, S. *Solid State Commun.* **2005**, *133*, 771.
(44) Bandoli, G.; Barreca, D.; Brescacin, E.; Rizzi, G. A.; Tondello, E. *Chem. Vap. Deposit.* **1996**, *2*, 238.
(45) Kang, S. W.; Rhee, S. W. *J. Electrochem. Soc.* **2003**, *150*, C573.
(46) Bedoya, C.; Condorelli, G.; Anastasi, G.; Baeri, A.; Scerra, F.; Fragala, I.; Lisoni, J.; Wouters, D. *Chem. Mater.* **2004**, *16*, 3176.
(47) Bedoya, C.; Condorelli, G. G.; Finocchiaro, S. T.; Di Mauro, A.; Fragalà, I. L.; Cattaneo, L.; Carella, S. *Chem. Vap. Deposit.* **2005**, *11*, 261.
(48) Moniz, S. J. A.; Blackman, C. S.; Carmalt, C. J.; Hyett, G. *J. Mater. Chem.* **2010**, *20*, 7881.
(49) Poleti, D.; Karanovic, L.; Zdujic, M.; Jovalekic, E.; Brankovic, Z. *Solid-State Sci.* **2004**, *6*, 239.
(50) Takeyama, T. *Opt. Mater.* **2004**, *26*, 413.
(51) Takeyama, T.; Takahashi, N.; Nakamura, T.; Itoh, S. *Mater. Res. Bull.* **2006**, *41*, 1690.
(52) Leontie, L.; Caraman, M.; Visinoiu, A.; Rusu, G. *Thin Solid Films* **2005**, *473*, 230.
(53) Putkonen, M.; Aaltonen, T.; Alnes, M.; Sajavaara, T.; Nilsen, O.; Fjellvag, H. *J. Mater. Chem.* **2009**, *19*, 8767.
(54) Myllymäki, P.; Roeckerath, M.; Lopes, J. M.; Schubert, J.; Mizohata, K.; Putkonen, M.; Niinistö, L. *J. Mater. Chem.* **2010**, *20*, 4207.
(55) Lie, M.; Fjellvag, H.; Kjekshus, A. *Thin Solid Films* **2005**, *488*, 74.
(56) Klepper, K. B.; Nilsen, O.; Fjellvag, H. *Thin Solid Films* **2007**, *515*, 7772.
(57) Elam, J. W.; Baker, D. A.; Martinson, A. B. F.; Pellin, M. J.; Hupp, J. T. *J. Phys. Chem. C* **2008**, *112*, 1938.
(58) Burton, B.; Goldstein, D.; George, S. *J. Phys. Chem. C* **2009**, *113*, 1939.
(59) Kuribayashi, K.; Ueyama, R. *Thin Solid Films* **1997**, *295*, 16.
(60) Maki, K.; Komiya, N.; Suzuki, A. *Thin Solid Films* **2003**, *445*, 224.
(61) Sung, M. M.; Kim, C.; G Kim, C.; Kim, Y. *J. Cryst. Growth* **2000**, *210*, 651.
(62) Aspinall, H. C.; Gaskell, J. M.; Loo, Y. F.; Jones, A. C.; Chalker, P. R.; Potter, R. J.; Smith, L. M.; Critchlow, G. W. *Chem. Vap. Deposit.* **2004**, *10*, 301.
(63) Burriel, M.; Garcia, G.; Santiso, J.; Abrutis, A.; Saltyte, Z.; Figueras, A. *Chem. Vap. Deposit.* **2005**, *11*, 106.